METALLURGICAL EVALUATION OF A DOT-E6498-2216 CYLINDER

FaAA Project No.: DC17916.000

Prepared for:

U.S. Department of Transportation
400 Seventh Street S.W.
Washington D.C. 20590

Prepared by:

Timothy R. Smith, Ph.D., P.E.
Failure Analysis Associates, Inc.
310 Montgomery Street
Alexandria, VA 22314

January 1997

TABLE OF CONTENTS

LIST OF FIGURES

1.0 Introduction

The U.S. Department of Transportation (DOT) contracted with Failure Analysis Associates, Inc. (FaAA) to perform a metallurgical examination of the remains of a failed aluminum cylinder. The cylinder, a DOT-E6498-2216 type[1] with serial number T127279 manufactured by Luxfer USA, was incorporated into a Scott Air Pak for fire-fighting use.

The scope of this investigation was to perform a detailed evaluation of the cylinder remains, including photodocumentation and non-destructive examinations, chemical and mechanical property determination, metallographic sectioning, and fractography. The detailed workscope for this evaluation is provided in Appendix A. This report presents the findings of this evaluation.

2.0 Visual Examination

A visual examination of the cylinder remains was performed. The remains are shown in Figure 1, in the as-received condition. The cylinder broke apart into four large pieces and at least two small fragments. At the time of FaAA's inspection, a circular sample of material had been cut from one piece and contained burn markings, presumably from tests by optical emission spectroscopy to determine its bulk chemistry. In addition, some aluminum chips, presumably from drilled holes at unknown location(s), were also included in the remains.

Stampings on the neck of the cylinder indicated that the first hydrostatic test on it was performed in 11/77. This is taken as its date of manufacture. Inspection stampings indicated that the cylinder had been pressure re-tested in 1982, 1988, and 1993. Further markings of "SCOTT" indicate the original equipment manufacturer of the air pak (not required by DOT); however, the aluminum cylinder was manufactured by Luxfer USA, per the E6498 exemption. A complete photodocumentation of the pieces was undertaken and is presented in Appendix B.

The fracture surfaces of the cylinder were inclined (i.e., non-radial with respect to the cylinder axis) shear-type, except in the neck region where the fracture surfaces were flat and radial with respect to the axis of the cylinder. The main fracture surface ran through essentially a full diameter of the inlet hole in the neck region. Figure 2 shows the matching halves of the fracture surface from the neck region (fragments 2A-1 and 2A-2). The larger of the two pieces (2A-1) had foreign contamination on the fracture surface on both sides of the inlet hole. This contamination appeared to be paint and either concrete dust or plaster. This piece also showed impact damage to the fracture surface at the inlet

[1] DOT E6498 is an exemption, dated 7/76, to the provisions of DOT's then-applicable Hazardous Materials Regulations granted to Luxfer, USA Ltd. to manufacture, mark and sell cylinders for the use in transportation in commerce of certain liquefied and nonliquefied compressed gases. This exemption satisfies the DOT-3Al section of 49 CFR-178.45.

hole, presumably a result of the pressurized cylinder rupture. Other pieces also showed impact damage at certain locations, all appearing to be from the rupture event.

Figure 3 shows two views of the fracture surface of fragment 2A-1 from the neck region. The inside wall of the cylinder in this region shows multiple folds (or cusps) from the original manufacturing process. The fracture surface on both sides of the inlet hole appears to pass through deep folds of this type. On fragment 2A-1, there were a least two large cracks, labeled SC1 and SC2 on Figure 3, originating from these folds.

3.0 Quantitative Chemical Analysis

A portion of the cylinder was removed and tested by optical emission spectrometry to determine the chemical composition. The results of this analysis are shown in Table 1 and indicate that the cylinder conforms to the Aluminum Association (AA) 6351 alloy specification and satisfies the DOT-E6498 specification for aluminum alloy chemistry.

Table 1: Chemistry of the Cylinder, Neck Region

	Composition (wt.%)		
Element	Test Result	AA6351 Specification (low)	AA6351 Specification (high)
Mg	**0.62**	**0.40**	**0.80**
Si	**0.96**	**0.70**	**1.30**
Ti	**0.03**	**0.00**	**0.20**
Mn	**0.60**	**0.40**	**0.80**
Fe	**0.22**	**0.00**	**0.50**
Cu	**0.01**	**0.00**	**0.10**
Zn	**0.01**	**0.00**	**0.20**
OE	**<0.05**	**0.00**	**0.05**
OT	**<0.15**	**0.00**	**0.15**
Al	**balance**	**balance**	**balance**

Chemical composition determined by optical emission spectrometry in accordance with the ASTM-E1019-94 standard. "OE" denotes "other elements", "OT" denotes the total of all "other elements" not listed in the table.

Samples of chips, taken using an electric drill from the neck, the sidewall, and the bottom of the cylinder, were dissolved in solution and analyzed by atomic absorption spectrometry to determine their chemical composition. The results are shown in Table 2.

Table 2: Chemistry of the Cylinder

Element	Composition (wt.%)				
	Test Result Neck	Test Result Side wall	Test Result Bottom	49 CFR-178.46-5 Specification (low)	49 CFR-178.46-5 Specification (high)
Mg	**0.73**	**0.68**	**0.65**	**0.40**	**0.80**
Si	**0.90**	**0.90**	**1.00**	**0.70**	**1.30**
Ti	**0.02**	**0.02**	**0.02**	**0.00**	**0.20**
Mn	**0.60**	**0.62**	**0.62**	**0.40**	**0.80**
Fe	**0.23**	**0.21**	**0.14**	**0.00**	**0.50**
Cu	**0.03**	**0.05**	**0.02**	**0.00**	**0.10**
Zn	**<0.02**	**<0.02**	**<0.02**	**0.00**	**0.20**
Bi	**<0.0050**	**<0.0050**	**<0.0050**	**0.00**	**0.01**
Pb	**<0.0040**	**<0.0040**	**<0.0050**	**0.00**	**0.01**
Al	**balance**	**Balance**	**balance**	**balance**	**balance**

Chemical composition determined by atomic absorption spectrometry in accordance with the ASTM-E663 and ASTM-D3335 standards.

These results show compliance with both the DOT exemption E6498 and the current DOT federal regulation 49 CFR 178.46-5, with no significant variations based on the sample location from within the cylinder. Note that the Pb levels found were below the detection threshold of 40 weight-ppm (5.2 atomic-ppm[2]). In addition, the Bi levels were below 50 weight-ppm (6.5 atomic-ppm).

4.0 Mechanical Testing

4.1 Tensile Testing

Standard size ASTM 370 tensile test coupons from the cylinder wall, aligned along the cylinder axis, were tested at room temperature. Fragment 2A-1 was sectioned, Figure 4(a), and component 2A-1C was used for tensile test coupons, as it contained material minimally deformed by the cylinder rupture. Three full-thickness coupons were chosen and Figure 4(b) shows them in the post-tested configuration. The test data are shown in Table 3.

The average values found are above the current 49 CFR 178.46-5 minimum specification and exceed the elongation requirement of E6498. They compare well with values of 42.8 ksi yield strength, 49.3 ksi ultimate strength and 13% elongation (2 inch gauge length), published for 6351 in T6 temper [1]. DOT E6498 requires that the material be AA6351-T6.

[2] calculated using the equation: atomic-ppm (Pb) = weight-ppm (Pb)*GMW(Al)/GMW(Pb); where GMW is the gram molecular weight of the element in parenthesis. The same equation was used for the bismuth level with Bi replacing Pb.

Table 3: Mechanical Properties

Test	Yield (ksi)	UTS (ksi)	Elongation (%)	49 CFR 178.46-5 Yield (min.) (ksi)	49 CFR 178.46-5 UTS (min.) (ksi)	Elongation (%)
2A-1C#1	**46.5**	**51.5**	**19.0**	**37.0**	**42.0**	**14**
2A-1C#2	**46.9**	**50.5**	**16.0**	**37.0**	**42.0**	**14**
2A-1C#3	**47.0**	**50.5**	**15.0**	**37.0**	**42.0**	**14**
Average	**46.8**	**50.8**	**16.7**	**37.0**	**42.0**	

Notes:
1. Tests were performed in accordance with the ASTM A370-77 Standard; gauge length was 2 inches.
2. Yield denotes the yield strength (0.2% offset), UTS denotes ultimate tensile strength.
3. Elongation values from the flat coupons tested here differ from the 49 CFR 178.46-5 values based on cylindrical specimens. E6498 requires a minimum elongation of 14% in either flat or cylindrical specimens.

4.2 Hardness Testing

Rockwell hardness measurements were made on a slice removed from the tank sidewall area of fragment 2A-2B (see Figure 5). A total of ten measurements was taken; the results are shown in Table 4.

Table 4: Hardness Measurements

Component	Indent No.	Hardness (Rockwell B)	Average Hardness (Rockwell B)
2A-2B1	1	58.3	59.4 HRB
	2	58.1	
	3	58.6	
	4	59.2	
	5	60.5	
	6	59.5	
	7	60.1	
	8	60.5	
	9	59.2	
	10	59.5	

Rockwell hardness measurements were made using a 100 kg load on a Leco RT-370 hardness tester.

5.0 Sectioning and Metallography

Figure 5 shows the sections cut from cylinder fragments 2A-2 and 2A-4. A section of the fracture surface was cut from cylinder fragment 2A-2 that removed the flat-faced portion on one side of the inlet hole. A wafer approximately 0.05 inch thick was generated ("FS" in Figure 5) in this process. The remaining piece was then sectioned in a parallel slice, as close as possible to the previous cut. This section was then polished and etched to reveal

its structure ("MET" in Figure 5). This polished metallurgical section should have a microstructure virtually identical to that at the fracture surface itself.

Figure 6(a) shows the wafer containing the fracture surface from Figure 5 and Figure 6(b) shows the etched macrostructure of the same region from the second wafer sliced parallel to the fracture surface. Some correspondence between features on the fracture surface and the grains is seen. Note that the grain size is relatively small, compared to the thickness at the neck.

Figure 7 shows the sectioning performed on fragment 2A-1 from the neck region. The cracks, SC1 and SC2 (Figure 3), were selected for further study. Crack SC1 was forced open in the laboratory, after the remaining ligament was saw-cut part way through. The newly-formed fracture surfaces are shown in Figure 7. Crack SC2 was sectioned just below the inlet hole threads (section 2A-1A2B) and metallurgically polished to reveal its morphology.

Figure 8 shows section 2A-1A2b containing crack SC2. Note the multiple folds at the inside surface and multiple branched cracks emanating from these folds. Figure 8(a) shows the section in the unetched condition and Figure 8(b) shows the microstructure after preparation with a $HF+H_2SO_4+H_2O$ etch. The microstructure is typical for AA6351 in the T6 temper condition. Figure 9 shows a higher magnification view of the crack marked "A" in Figure 8. Note that the main crack degenerates into multiple fine-scale branches.

Figure 10 shows the tip of a crack from the subject cylinder that was examined metallographically. Note that the crack appears to be discontinuous. Formation of the crack also appears to be associated with Mg_2Si and AlFeSi compounds in the microstructure, shown as the distributed darker grey phases in Figure 10. To determine if the cracks were associated with a particular type of inclusion, a polished metallographic section was examined in the scanning electron microscope (SEM) and the chemical composition of the inclusions probed by energy dispersive spectroscopy (EDS). Figure 11 shows the results of this analysis. Note that the majority of inclusions seen in this micrograph (such as A and C) contain Fe and Mn, and thus are expected to be of the AlFeSi type, a variant of which also contains Mn substitutionally for Fe [2]. Inclusion B, with strong Mg and Si peaks, appears to be Mg_2Si. While not conclusive, Figure 10 and 11 suggest that the cracks form along stringers of AlFeSi compounds.

6.0 Fractography

The wafer containing the flat-faced fracture surface shown in Figure 6 was examined optically and in the scanning electron microscope (SEM). The optical examination revealed that the flat-faced (i.e., planar and radial with respect to the cylinder axis) region of the fracture surface shows little macroscopic ductility. Just outside of this region, the fracture surface transitioned to an inclined (i.e., non-radial with respect to the cylinder

axis) shear-type of fracture. The region just below the inlet hole threads and close to the inside of the cylinder contained some of the chromate coating[3] used to line the cylinder, suggesting that a deep fold was present at this location at the time of manufacture. This finding is consistent with the metallographic sectioning.

Fractography of the wafer also shows an apparent beach mark (see Figure 6) in the flat-faced region. SEM fractographs taken from inside and beyond this beach mark, however, fail to provide a clear distinction in the failure mode between these two regions. Figure 12 shows a series of SEM fractographs taken from this fracture surface. Region 1 (Figure 12a) was from near the inside of the tank, close to the threads at the inlet hole. Higher magnification view of region 1 are shown in Figure 12(b) and (c). This region contains a mixture of intergranular and transgranular fracture, with very fine-scale dimples on the faceted surfaces. In region 2 (Figure 12a), in the flat-faced region, the fracture surface contains larger-scaled dimples but still contains intergranular facets with very fine-scale dimples. SEM fractographs of this region are shown in Figure 12 (d) and (e). Region 3 (Figure 12a) is in the shear-lipped region outside of the flat-faced portion of the fracture. This region shows predominantly dimpled rupture, Figure 12(f) and (g). Figure 13 shows energy dispersive spectroscopy (EDS) surface chemistry results captured from region 1 (near to the inlet hole threads) and region 2 (on the flat-faced fracture away from the inlet hole). The presence of oxygen in region 1, as compared to region 2, suggests that region 1 formed earlier. This is consistent with the flat oxidized appearance of the fracture surface in region 1. These spectra also show chromium (Cr), silver (Ag), calcium (Ca), and chloride (Cl) contamination. The Cr and Ag are likely from the exterior paint and/or the chromate interior coating, perhaps deposited during solvent cleaning of the remains.

Figure 14 shows fractographs of the crack SC2 (see Figures 3 and 7) that was forced open in the laboratory. Figure 14(a) and (b) show matching halves of the fracture surface. Three distinct regions are apparent: region 1, a flat-faced region near to the cylinder's inside surface at the inlet hole; region 3, a similar flat-faced region near to the cylinder's outside surface at the inlet hole; and region 2, a curved fracture surface joining regions 1 and 3. Figure 14 (c)-(j) are a series of SEM fractographs from regions 1 - 3 described above, and from region 4, (see Fig. 12a), close to the extremity of the crack prior to it being forced open. Figure 15 shows EDS spectra captured from the fracture surface (as shown in Figure 12) from regions 1 - 4. Note Ag and Ca contaminants in region 2, similar to those found on the original fracture surface (see Figures 12 and 13).

Figure 16 shows SEM fractographs of the fracture surface from one of the tensile specimens (specimen 2A-1C1, Figure 4) used for mechanical property determination. Note that the fracture surface is primarily ductile dimpled rupture, with both macro and micro dimples, and some intergranular faceting, with microdimpling on these facets. This morphology is consistent with fractographic studies of similar Al alloys in tensile and toughness testing [3]. A comparison of the Figure 16 fractographs with Figures 12

[3] the coating on the inside of the cylinder was determined to be of a chromate type, based on an energy dispersive spectroscopy (EDS) analysis of it (spectra not shown).

and 14, indicates that there is no clear differentiation fractographically between tensile overload and a large portion of the flat-faced fracture surfaces, described above.

7.0 Discussion

Examination and testing of the cylinder remains demonstrates that the subject cylinder meets the chemical and mechanical property requirements of DOT E6498 and current DOT 49 CFR 178.46. Both lead (Pb) and bismuth (Bi) are below the regulation limits specified in both E6498 and 49 CFR 178.46-5. The composition of the alloy indicates that it complies with the Aluminum Association specification for AA6351-T6 in accordance with E6498. The microstructure appears to be typical for this alloy and heat treatment.

Examination of the fracture surfaces of each cylinder fragment suggests that the failure originated from the neck region of the cylinder near to the inlet hole. The flat-faced (i.e., radial) nature of the fracture surface at the neck region with little macroscopic ductility followed by a transition to an inclined (i.e., non-radial) shear-type of fracture on both sides of the cylinder, suggests fast fracture, originating from the flat-faced region on both sides of the inlet hole prior to final rupture. It is clear from Figures 2 and 3 that a sub-critical crack of some size existed on each side of the inlet hole. Both of these sub-critical cracks grew and were incorporated into the fracture surface. It is not clear if one or both of these cracks had reached critical size at the time of rupture.

The location of a beach mark on the fracture surface segment studied in detail (Figures 6 and 12) suggests that this crack propagated sub-critically (i.e., slowly) for the majority of the flat-faced region up to the extent defined by the beach mark. A similar, but perhaps less defined beach mark is present on the opposite side of the inlet hole. These beach marks are consistent with the morphology of cracked regions at the neck of other DOT-6498, DOT-3Al, and DOT-7235 aluminum cylinders that were rejected during hydrostatic retesting [4] and with an Australian-specification aluminum cylinder that leaked during filling [5]. This morphology is also consistent with the fracture surface of a DOT-3AL cylinder that ruptured during filling, provided for FaAA's examination by J. H. Smith of the National Institute of Science and Technology [6].

Sectioning of the cylinder wall just below the threads at the inlet hole revealed multiple cracks from multiple origins at folds (or cusps) in the inside wall. These branched cracks are consistent with cracks found in the neck region of other DOT-6498, DOT-3Al, and DOT-7235 aluminum cylinders [4]. The possible association of cracks with AlFeSi compounds in the microstructure of the subject cylinder is consistent with other reported work on intergranular creep embrittlement of Al-Mg-Si alloys [3]. In this regard the observed cracks are consistent with studies of "sustained-load cracking" at ambient temperature reported in the literature for similar Al alloys [3, 7-9, 10-11].

8.0 Summary and Conclusions

A metallurgical examination of an aluminum cylinder DOT-E6498-2216 type, with serial number T127279 showed the following results.

- This 1977-vintage cylinder meets the chemical specifications of the E6498 exemption and the current 49 CFR 178.46-5 for AA6351 alloy, including lead (Pb) and bismuth (Bi) levels.
- This 1977-vintage cylinder meets the mechanical property specifications of the E6498 exemption and of the current 49 CFR 178.46-5 and 178.46-13.
- Multiple cracks were found originating at folds in the interior wall in the neck region near the inlet hole. These folds were associated with the cylinder's manufacture.
- Cracks showed a multiple-branched morphology; crack tips appeared to be discontinuous.
- The cylinder failed from the neck region when a sub-critical crack in the neck region grew to critical size. The primary fracture surfaces developed from cracks at folds on the interior wall.
- Fracture surfaces were not associated with the neck threads.
- The apparent origin of the fracture is consistent with sustained-load cracks reported in the literature for similar Al alloys. The crack size at the time of rupture appears to be defined by the macroscopic beach marks on the flat-faced (i.e., radial) portions of the fracture surface.

9.0 References

1. J. E. Hatch, Ed., (1984). Aluminum: Properties and Physical Metallurgy, American Society for Metals, Metals Park, OH, p. 363.

2. ASM Metals Handbook, 9th. Ed., Vol. 9, "Metallography and Microstructures", American Society for Metals, Metals Park, OH, p. 356.

3. M. Guttmann, B. Quantin, and Ph. Dumoulin (1983). "Intergranular creep embrittlement by non-soluble impurity: Pb precipitation hardened Al-Mg-Si alloys", Metal Sci., Vol. 17, No. 3, pp. 123-140.

4. J. H. Smith (1987). "Evaluation of Cracking in Aluminum Cylinders", NBSIR 86-3492, Institute for Materials Science and Engineering, National Bureau of Standards (NBS), U.S. Dept. of Commerce, Gaithersburg, MD.

5. J. W. H. Price, R. N. Ibrahim and D. Ischenko (1996). "Cracking in Aluminum 6061 and 6351 Gas Cylinders", Proc. Int. Conf. on Pressure Vessel Technology, Vol 1., American Society of Mechanical Engineers (ASME), Montreal, Canada, pp. 337-343.

6. per. com., J. H. Smith (1996), Materials Science and Engineering Laboratory, National Institute of Standards and Technology (NIST), U.S. Dept. of Commerce, Gaithersburg, MD.

7. J. J. Lewandowski, Y. S. Kim, and N. J. H. Holroyd (1992). "Lead-Induced Solid Metal Embrittlement of an Excess Silicon Al-Mg-Si Alloy at Temperatures of -4°C to 80° C", *Met. Trans. A.*, Vol. 23A, pp. 1679-1689.

8. Y. S. Kim, N. J. H. Holroyd, and J. J. Lewandowski (1989). "Pb-Induced Solid-Metal Embrittlement of Al-Mg-Si Alloy at Ambient Temperatures", *Proc. Environment-Induced Cracking of Metals.*, National Association of Corrosion Engineers (NACE), pp. 371-377.

9. J. J. Lewandowski, V. Kohler, and N. J. H. Holroyd (1987). "Effects of Lead on the Sustained-load Cracking of Al-Mg-Si Alloys at Ambient Temperatures", *Mat. Sci & Eng.*, Vol. 96, pp. 185-195.

10. H. L. Stark and R. N. Ibrahim (1992). "Crack Propagation in Aluminum Gas Cylinder Neck Material at Constant Load and Room Temperature", Eng. Fracture Mechanics, Vol. 41, No. 4, pp. 569-575.

11. H. L. Stark and R. N. Ibrahim (1988). "Crack Propagation at Constant Load and Room Temperature in an Extruded Aluminum", Eng. Fracture Mechanics, Vol. 30, No. 3, pp. 409-414.

Figure 1. Remains of the cylinder, as received.
Photo ID: DC17916-R4E6.

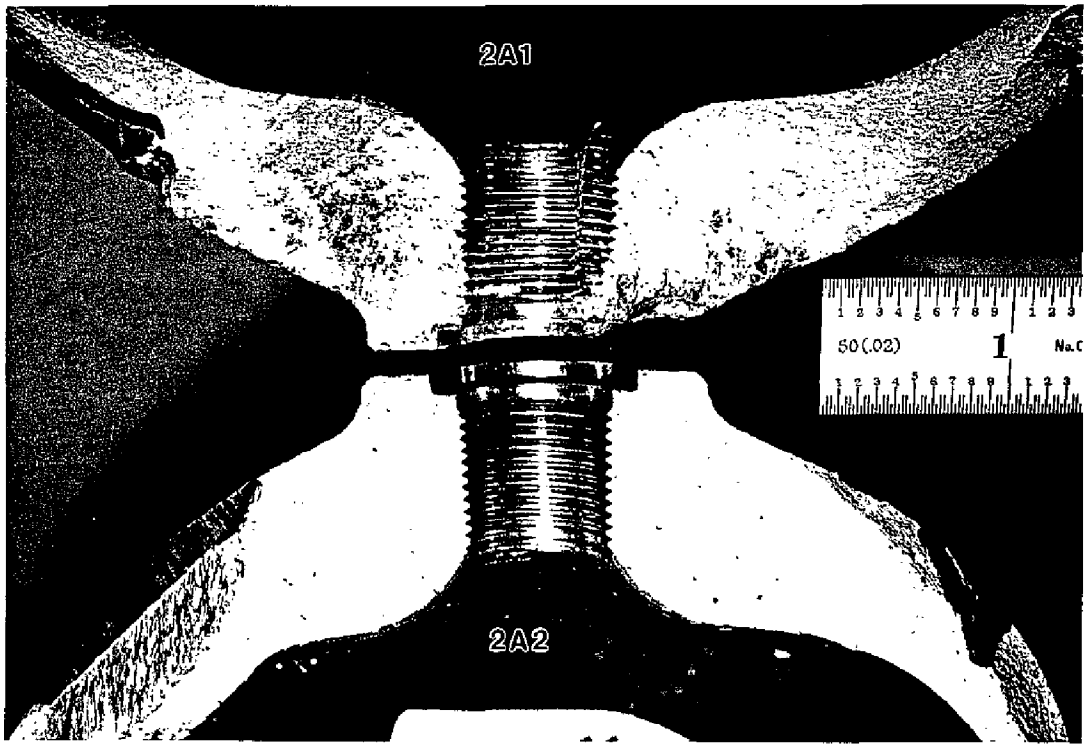

Figure 2. Mating fracture surfaces (fragments 2A-1 and 2A-2) at the inlet hole. Note the fracture is planar in the neck region.
Photo ID: DC17916-R5E5.

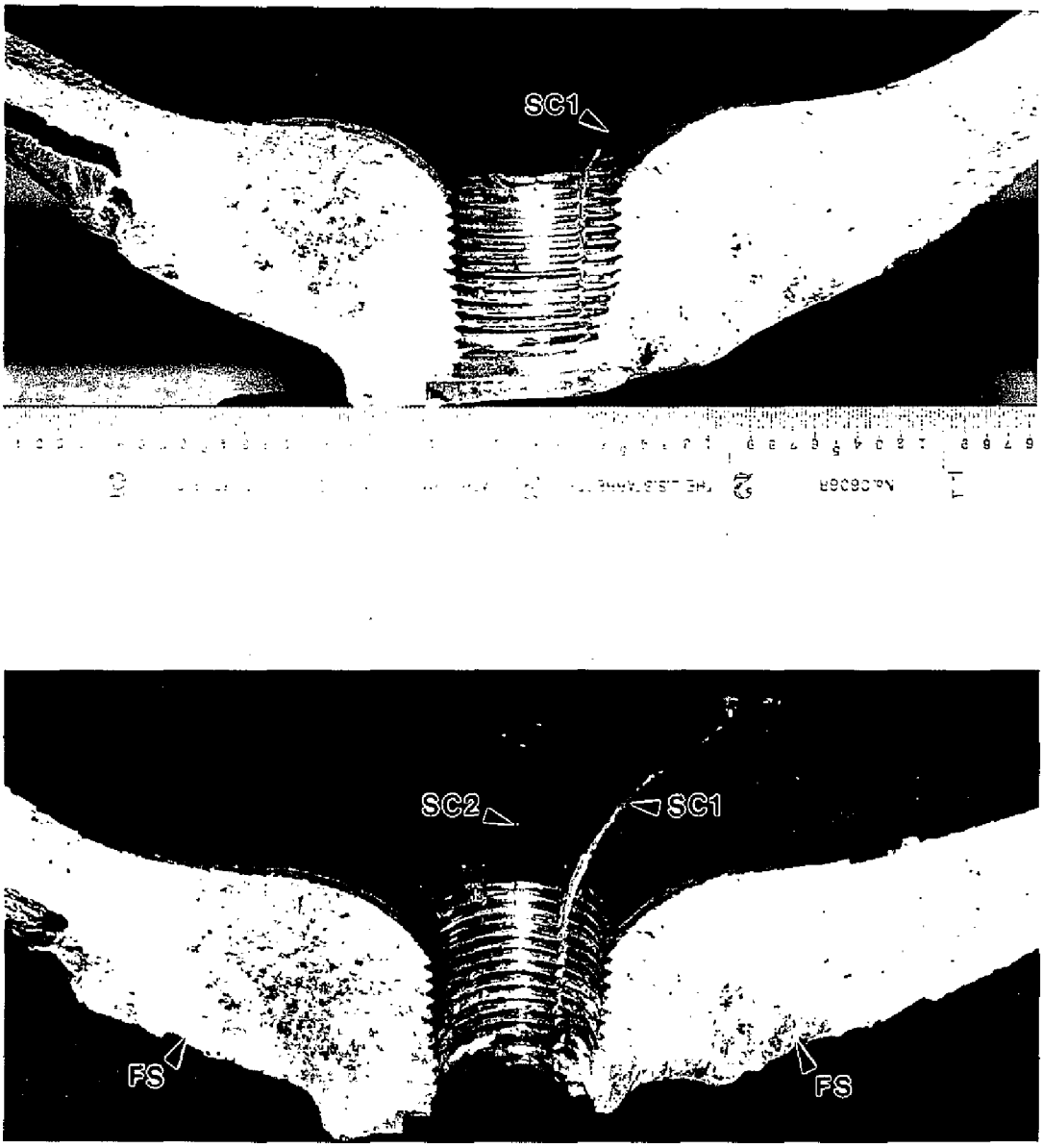

Figure 3. Fragment 2A-1 fracture surface, neck region.
(a) View perpendicular to fracture surface.
Photo ID: DC17916-R4E20.
(b) View inclined to fracture surface.
Photo ID: DC17916-R4E21.
Note: FS marks the fracture surface, SC1 and SC2 are secondary cracks.